Pergamon

Int. J. Heat Mass Transfer. Vol. 41, No. 2, pp. 411–423, 1998

Printed in Great Britain
0017-9310/98 $19.00+0.00

PII: S0017-9310(97)00122-1

Mixed convection heat transfer in horizontal rectangular ducts with wall transpiration effects

KUAN-TZONG LEE

Department of Mechanical Engineering, Oriental Institute of Technology, Pan-Chiao, Taipei, Taiwan 22064, Republic of China

and

WEI-MON YAN

Department of Mechanical Engineering, Hua Fan College of Humanities and Technology, Shih-Ting, Taipei, Taiwan 22305, Republic of China

(*Received* 14 *August* 1996 *and in final form* 18 *April* 1997)

Abstract—A detailed numerical study was carried out to examine the effects of wall transpiration on laminar mixed convection flow and heat transfer in the entrance region of horizontal rectangular ducts. The vorticity–velocity method was employed in the formulation. Both thermal boundary conditions of uniform heat flux (UHF) and uniform wall temperature (UWT) were considered. Predicted results are presented for air flow over a wide range of governing parameters. In this work, the wall Reynolds number Re_w are varied from -2 (suction) to 4 (injection) with Rayleigh numbers Ra ranging from 0 to 2×10^5 for aspect ratios $\gamma = 0.2$, 0.5, 1, 2 and 5. The predicted results show that either wall injection or wall suction has a considerable impact on the flow structure and heat transfer performance. In addition, the correlating equations for the average fRe and Nu are presented. © 1997 Elsevier Science Ltd.

INTRODUCTION

The problems of convection heat transfer in a porous-wall duct with wall injection or suction are encountered in certain heat-transfer problems. For instance, when hot fluid flows through the channel, problems which arise form flowing fields to solid boundaries must be inhibited so that the surface temperature do not exceed design limit. The problems of overheating of wall may be overcome by the injection of fluid through the walls. Methods to decreasing rates of heat transfer may become important in combustion chamber, exhaust nozzles and porous walled flow reactors. Other engineering applications includes turbine engines, solar energy collectors, electrochemical systems, fuel cell stacks, heat pipes and food-drying processes. Although there are a larger number of publications dealing with various combination of channel flow in porous ducts with suction or injection flow, the buoyancy effects on the momentum and heat transfer characteristics has not been investigated.

To gain perspective of wall transpiration effects, the problems of fully developed parallel-plate flow are first briefly reviewed. Berman [1] and Donoughe [2] obtain a similarity solution for a two-dimensional duct. They successfully solved the governing momentum equations with small wall transpiration by using the perturbation technique. Carter and Gill [3] investigated the effects of wall transpiration on combined forced and free convection in vertical and horizontal channels. Terrill [4] obtained a singular perturbation solution for slow flow through the channel of the case of suction at one wall and equal blowing at the other wall. Heat transfer in porous duct flow has been investigated by Yeroshenko *et al.* [5]. In their results, they generalised a single relation in the form of the relative heat transfer law for all Prandtl number.

The study of developing flow in parallel-plate channel has been examined by numerous researchers. Calculations of heat transfer for the thermal entrance region of two-dimensional channel, with hydrodynamic flow stabilization, were obtained by a finite-difference method in refs. [6, 7]. The influence of variable property of fluid on heat transfer in a two-dimensional flat channel was studied in ref. [8]. Their results showed that the Nusselt number will increase for flow with injection through thermal entry region over the constant property value for the same wall Reynolds number. Raithby and Knudsen [9] solving the two-dimensional, elliptical equations of the motion for the development of laminar flow. They concluded that the flow cannot be fully developed for high suction rate. Tsou and Chang [10] gave the analytical solution of linearized motion and energy equations as a series of eigenfunctions in terms of hypergeometrical functions. Rhee and Edwards [11]

NOMENCLATURE

A cross-sectional area of the rectangular duct [m^2]
a, b width and height of the rectangular duct, respectively [m]
$\bar{a}, \bar{b}, \bar{c}, \bar{d}, \bar{e}, \bar{f}$ constants of correlating equations
D_e equivalent hydraulic diameter, $4A/S$
f friction factor, $2\bar{\tau}_w/(\rho\bar{w}_0^2)$
h circumferentially averaged heat transfer coefficient [$W\ m^{-2}\ K^{-1}$]
k thermal conductivity [$W\ (mK)^{-1}$]
M, N number of finite difference divisions in the X- and Y-directions, respectively
n dimensionless direction coordinate normal to the duct wall
Nu local averaged Nusselt number, hD_e/k
p pressure [$N\ m^{-2}$]
p_0 hydrostatic pressure [$N\ m^{-2}$]
$\bar{P}$ dimensionless averaged pressure over the cross-section of the duct
P' dimensionless perturbation pressure about the mean pressure $\bar{P}$
Pr Prandtl number, ν/α
Ra Rayleigh number, $g\beta\Delta TD_e^3/(\nu\alpha)$
Re_0 inlet Reynolds number, $\bar{w}_0D_e/\nu$
Re_w wall Reynolds number, $v_{in}D_e/\nu$, positive for injection flow and negative for suction flow
S circumference of cross-section [m]
T temperature [K]
u, v, w velocity components in the x-, y- and z-directions, respectively [$m\ s^{-1}$]
U, V, W dimensionless velocity components in the x-, y- and z-directions, respectively, $=uD_e/\nu, vD_e/\nu, w/\bar{w}_0$
v_{in} magnitude of fluid velocity injected or suctioned through the porous wall [$m\ s^{-1}$]
$\bar{w}_0$ mean velocity at the inlet [$m\ s^{-1}$]
$\bar{W}$ dimensionless mean velocity [$m\ s^{-1}$]
x, y, z coordinate system [m]
X, Y, Z dimensionless coordinate system, $=x/(D_e), y/(D_e), z/(D_eRe_0)$
Z^* dimensionless axial coordinate, Z/Pr.

Greek symbols

α thermal diffusivity [$m^2\ s^{-1}$]
γ aspect ratio, a/b
ξ dimensionless vorticity in the z-direction
θ dimensionless temperature, $(T-T_0)/\Delta T$
ν kinematic viscosity [$m^2\ s^{-1}$]
ρ fluid density [$kg\ m^{-3}$]
τ_w shear stress [$N\ m^{-2}$]
ΔT characteristic temperature difference, q''_wD_e/k for UHF or (T_w-T_0) for UWT.

Subscripts

b bulk fluid quantity
w value at wall.
0 condition at inlet or condition without buoyancy (i.e. $Ra = 0$).

analysed a simultaneous thermally and hydrodynamically developing flow in a long, uniform, semi-porous duct. Lessner and Newman [12] developed a high Reynolds number and high Schmidt number singular perturbation expansion for the semi-porous duct. Sorour *et al.* [13] suggested that a large inlet suction rate is recommended for hydrodynamic applications and a small inlet suction is recommended for heating applications. Yuan and Finkelstein [14] investigated the laminar flow in a porous-wall pipe by the solution of Navier–Stokes equations in cylindrical coordinate. They expanded the dimensionless stream function in a Taylor series in which wall Reynolds number, based on wall velocity, was the expansion parameter. Their results showed that the friction factor was increased by 70–85% over the zero injection case for injection Reynolds number in the range $500 \leqslant Re_w \leqslant 2500$.

The heat transfer in porous tube in the region of fully developed flow has received considerable attention. Olson and Eckert [15] investigated experimentally the effects of injection on mixing length and eddy diffusivity of turbulent flow. Their results showed the normalised friction factors agreed with values measured in external flow and the normalised velocity defect profiles with injection agreed with those for flow without injection. Kinney [16] carried out the calculations of stabilised heat transfer of fully developed laminar flow in a porous tube. He obtained the universal wall-friction and heat transfer results for flow in constant temperature tube. Bundy and Weissberg [17] presented data of overall pressure drop for wall injection, and found good agreement with fully developed solution in the range $0 < Re_w < 7.0$. Yeroshenko *et al.* [18, 19] presented the results of mean and fluctuation heat transfer characteristics in a turbulent flow. Their results indicated that the Stanton number for a region far from the inlet are well correlated to give a relative heat transfer law. Hirata and Ito [20] concluded that the mixing length near wall is increased by injection and decreased by suction, and the mixing length in the core region is decreased by injection and increased by suction.

The heat transfer in porous tube in the developing

region are available in the literature [21–25]. Yuan and Finkelstein [21] presented some entrance region heat transfer results that restricted to asymptotically small values of the wall injection. Pederson and Kinney [22] extended the work of Kinney [16] to the thermal entrance region in a porous channel for various thermal boundary conditions. Raithby [23] solved the energy equation by the Fourier methods. He also obtained a number of asymptotic expressions of the solution of strong injection. Raithby [24] provided the solution of arbitrary prescribed temperature or heat flux boundary conditions for tube and parallel-plate channel. The experimental results of Hirata *et al.* [25] revealed that the flow becomes fully developed up to the tube center at the axial location greater than 13 times of tube diameter. They also proposed a simple expression of defect law for velocity distribution in the core region.

For the flow in annulus, Faghri [26] numerically investigated the simultaneously developing velocity and temperature fields in the entrance region on annular passage. He observed that there is little or no tendency of obtaining fully developed behaviors for suction cases due to complete mass extraction. Raptis *et al.* [27] derived expressions of axial velocity, the volume of fluid flowing and stress component for two co-axial circular cylinders with small suction and injection.

The fluid flow and heat transfer in rectangular duct with porous walls has received attention recently. Hwang *et al.* [28] presented a numerical forced convection heat transfer and fluid flow in the entrance region of a square duct with one-walled injection and suction. Recently, Cheng and Hwang [29] conducted an experimental study to investigate the same problem. They found that the wall transpiration has a significant effect on the heat transfer and fluid flow in the entrance region of porous duct, but the buoyancy effect still remains untreated. The study of mixed convection in the horizontal duct without wall transpiration effects has been studied by numerous researchers [30–34]. They showed that the buoyancy effect has a significant impact on characteristics of flow structure and heat transfer performance.

Since the problem of the flow through a porous-wall rectangular duct with buoyancy effects has not been investigated thoroughly. The purpose of this work is to obtain the basic phenomena of this type flow which provide guidance for the investigation of mixed convection flow with wall transpiration effect. Both flow and heat transfer characteristics in developing laminar entrance region are numerically studied.

ANALYSIS

Consider the steady, laminar, developing flow in a heated horizontal rectangular duct with uniform wall injection or wall suction (Fig. 1). A uniform inlet axial velocity $\bar{w}_0$ and a constant inlet temperature T_0 are imposed at $z = 0$. The duct walls are subjected to either uniform wall heat flux (UHF) or uniform wall temperature (UWT). The temperature of the injected or suctioned fluid is the same as that of the duct wall. The u, v and w are the velocity components in the x-, y- and z-directions, respectively. In this work, the fluid is assumed to be constant thermophysical properties except the density variation in the buoyancy term in momentum equation. The Boussinesq approximation is invoked for the consideration of thermal buoyancy.

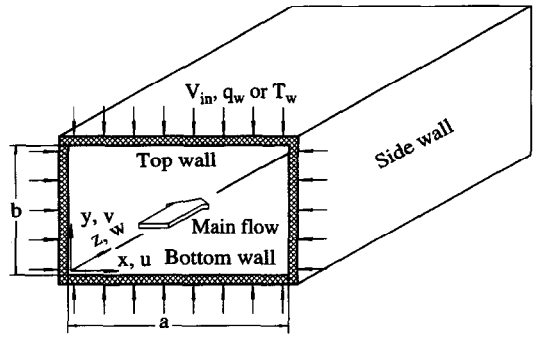

Fig. 1. Schematic diagram of the physical model.

Referring to the coordinate system shown in Fig. 1 and introducing the following dimensionless variables and parameters:

$$X = x/D_e \quad Y = y/D_e \quad Z = z/(Re_0 D_e)$$
$$Z^* = Z/Pr \quad U = uD_e/\nu \quad V = vD_e/\nu$$
$$W = w/\bar{w}_0 \quad P = \bar{p}/(\rho \bar{w}_0^2) \quad P' = p'/(\rho \nu^2/D_e^2)$$
$$Re_w = v_{in} D_e/\nu \quad Ra = g\beta \Delta T D_e^3/(\alpha\nu) \quad Pr = \nu/\alpha$$
$$\gamma = a/b \quad D_e = 4A/S \quad Re_0 = \bar{w}_0 D_e/\nu$$
$$\theta = (T - T_0)/\Delta T \quad \Delta T = q''_w D_e/k \quad \text{for UHF}$$
$$\text{or} \quad (T_w - T_0) \quad \text{for } UWT \tag{1}$$

the following dimensionless governing equations can then be obtained:

continuity equation

$$\frac{\partial U}{\partial X} + \frac{\partial V}{\partial Y} + \frac{\partial W}{\partial Z} = 0 \tag{2}$$

x-direction momentum equation

$$U\frac{\partial U}{\partial X} + V\frac{\partial U}{\partial Y} + W\frac{\partial U}{\partial Z} = -\frac{\partial P'}{\partial X} + \frac{\partial^2 U}{\partial X^2} + \frac{\partial^2 U}{\partial Y^2} \tag{3}$$

y-direction momentum equation

$$U\frac{\partial V}{\partial X} + V\frac{\partial V}{\partial Y} + W\frac{\partial V}{\partial Z} = -\frac{\partial P'}{\partial Y} + \frac{\partial^2 V}{\partial X^2} + \frac{\partial^2 V}{\partial Y^2} + \frac{Ra}{Pr}\theta \tag{4}$$

z-direction momentum equation

$$U\frac{\partial W}{\partial X} + V\frac{\partial W}{\partial Y} + W\frac{\partial W}{\partial Z} = -\frac{d\bar{P}}{dZ} + \frac{\partial^2 W}{\partial X^2} + \frac{\partial^2 W}{\partial Y^2} \tag{5}$$

energy equation

$$U\frac{\partial\theta}{\partial X}+V\frac{\partial\theta}{\partial Y}+W\frac{\partial\theta}{\partial Z}=\frac{1}{Pr}\left[\frac{\partial^2\theta}{\partial X^2}+\frac{\partial^2\theta}{\partial Y^2}\right]. \quad (6)$$

In writing the above equations, the axial diffusion terms of the momentum equations and the energy equation are neglected due to the assumptions of high Reynolds and Peclet numbers [35]. Additionally, the concept of motion pressure or pressure defect was introduced

$$p(x,y,z)=p_0+\bar{p}(z)+p'(x,y) \quad (7)$$

where p_0 is the hydrostatic pressure, $\bar{p}(z)$ the mean pressure over the cross-section, and $p'(x,y)$ the pressure deviation in the transverse direction.

A vorticity–velocity method developed by Ramakrishna *et al.* [36] is employed in this work. To constructed the vorticity–velocity formulation of the problem considered, a dimensionless axial vorticity is defined as

$$\xi=\frac{\partial U}{\partial Y}-\frac{\partial V}{\partial X}. \quad (8)$$

The axial vorticity transport equation can then be derived from equations (3) and (4) as

$$U\frac{\partial\xi}{\partial X}+V\frac{\partial\xi}{\partial Y}+W\frac{\partial\xi}{\partial Z}+\xi\left(\frac{\partial U}{\partial X}+\frac{\partial V}{\partial Y}\right)+\frac{\partial W}{\partial Y}\frac{\partial U}{\partial Z}$$
$$-\frac{\partial W}{\partial X}\frac{\partial V}{\partial Z}=\frac{\partial^2\xi}{\partial X^2}+\frac{\partial^2\xi}{\partial Y^2}-\frac{Ra}{Pr}\frac{\partial\theta}{\partial X}. \quad (9)$$

Equations for transverse velocity components (U, V) can be derived from the continuity equation, equation (2), and the definition of axial vorticity, equation (8), as

$$\frac{\partial^2U}{\partial X^2}+\frac{\partial^2U}{\partial Y^2}=\frac{\partial\xi}{\partial Y}-\frac{\partial^2W}{\partial X\partial Z} \quad (10)$$

$$\frac{\partial^2V}{\partial X^2}+\frac{\partial^2V}{\partial Y^2}=-\frac{\partial\xi}{\partial X}-\frac{\partial^2W}{\partial Y\partial Z}. \quad (11)$$

An additional constraint to deduce the axial pressure gradient is the global mass conservation. The expression is

$$\bar{W}=1+2Re_w\frac{(1+\gamma)^2}{\gamma}Z \quad (12)$$

where Re_w is the wall Reynolds number based on the injection or suction velocity v_{in}. For injection case, the Re_w is positive, while for suction case the Re_w is negative.

The problem is subjected to the following boundary conditions:

at the entrance $Z=0$: $W=1, U=V=\xi=0, \theta=0$

on the left wall $X=0$:

$$W=0, U=Re_w, V=0, \partial\theta/\partial Y=-1 \text{ (for UHF)}$$
$$\theta=1 \text{ (for UWT)}$$

on the right wall $X=(1+\gamma)/2$:

$$W=0, U=-Re_w, V=0, \partial\theta/\partial Y=1 \text{ (for UHF)}$$
$$\theta=1 \text{ (for UWT)}$$

on the bottom wall $Y=0$:

$$W=0, U=0, V=Re_w, \partial\theta/\partial X=-1 \text{ (for UHF)}$$
$$\theta=1 \text{ (for UWT)}$$

on the top wall $Y=(1+\gamma)/(2\gamma)$:

$$W=0, U=0, V=-Re_w, \partial\theta/\partial X=-1 \text{ (for UHF)}$$
$$\theta=1 \text{ (for UWT)}. \quad (13)$$

After the developing velocity and temperature fields are obtained, the computations of the circumferentially averaged friction factor parameter, fRe, and Nusselt number, Nu, are of practical interest. Following the usual definitions, the expression for the product of the peripherally averaged friction factor and Reynolds number fRe can be written based on the axial velocity gradient on the duct wall.

$$fRe=-2(\overline{\partial W/\partial n})_w. \quad (14)$$

Similarly, local averaged Nusselt number can also be evaluated from the average temperature difference between the duct walls and the bulk fluid temperature

$$Nu=\frac{1}{\overline{\theta_w}-\theta_b} \text{ for UHF} \quad (15)$$

$$Nu=\frac{(\overline{\partial\theta/\partial n})_w}{1-\theta_b} \text{ for UWT} \quad (16)$$

where the overbar means the average around the perimeters and n denotes the dimensionless coordinate normal to the duct wall. The bulk fluid temperature θ_b is defined as

$$\theta_b=\frac{\int_0^{\frac{1+\gamma}{2\gamma}}\int_0^{\frac{1+\gamma}{2}}\theta W\,dX\,dY}{\int_0^{\frac{1+\gamma}{2\gamma}}\int_0^{\frac{1+\gamma}{2}}W\,dX\,dY}. \quad (17)$$

SOLUTION METHOD

The governing equations are numerically solved by the vorticity–velocity method for three-dimensional parabolic flow [32]. For a given combination of governing parameters, Re_w, Ra, γ and Pr, the solution is evaluated by a marching technique based on the Dufort–Frankel scheme [37]. Details of the solution procedure have been described elsewhere [32–34], and not repeated herein.

To obtain enhanced accuracy, the grid line was uniformly arranged in the cross-plane but non-uniformly distributed in the axial direction to account

Table 1. Comparisons of local Nusselt number Nu for various grid arrangements for the case of $Re_w = -2.0$, $Ra = 1 \times 10^5$ and $\gamma = 1$ (UHF)

$M \times N$ / ΔZ^*	Z^* 0.001	0.01	0.02	0.04	0.06	0.08	0.1
21×21 $(1.5 \times 10^{-5} - 5 \times 10^{-4})$	12.970	5.7047	4.8986	4.9282	4.4977	4.2596	3.9352
41×41 $(1.5 \times 10^{-5} - 5 \times 10^{-4})$	15.384	6.1330	5.2016	5.4105	5.1275	5.0646	5.0033
61×61 $(1.5 \times 10^{-5} - 5 \times 10^{-4})$	15.800	6.1679	5.2135	5.4322	5.1369	5.0947	4.9948
41×41 $(3 \times 10^{-5} - 1 \times 10^{-3})$	15.278	6.0902	5.1722	5.4161	5.0865	5.0576	4.9058
41×41 $(7 \times 10^{-6} - 2.5 \times 10^{-4})$	15.412	6.1154	5.1876	5.3784	5.1003	5.0223	4.9649

for the uneven variations of velocity and temperature in the entrance region. Numerical experiments were carried out to ensure the independence of the results on the grid spacing and axial step sizes. Table 1 presents the results of the local Nusselt number Nu for the typical case with $Re_w = -2.0$, $Ra = 1 \times 10^5$ and $\gamma = 1.0$. It is clear in Table 1 that the deviations in Nu calculated with either $M \times N = 41 \times 41$ or 61×61 $(\Delta Z^* = 1.5 \times 10^{-5} - 5 \times 10^{-4})$ are always within 1%, except the axial location $Z^* = 0.001$. Furthermore, the deviations in Nu calculated using $M \times N(\Delta Z^*) = 41 \times 41(1.5 \times 10^{-5} - 5 \times 10^{-4})$ or $41 \times 41(7 \times 10^{-6} - 2.5 \times 10^{-4})$ are less than 1%. Accordingly, the computations involving a $M \times N(\Delta Z^*) = 41 \times 41(1.5 \times 10^{-5} - 5 \times 10^{-4})$ grid are considered to be sufficiently accurate to describe the mixed convection flow and heat transfer in a horizontal rectangular duct with wall transpiration effects. All the results presented in the next section are computed using the latter grid.

As a partial verification of the computational procedure, results were initially obtained for laminar mixed convection in a horizontal rectangular duct without wall transpiration effects. The results of heat transfer coefficient and friction factor were compared with those of Chou and Hwang [32]. The Nusselt number and friction factor were found to agree within 2% between the present predictions and those of Chou and Hwang [32]. In addition, the hydrodynamically developing flow without mass injection was calculated. These results are compared with those of Shah and London [35]. It was found that the differences in the fanning friction factor are within 1%. To further validate the numerical scheme used, the result was obtained for forced convection in an one-porous-wall square duct with various injected rate. The circumferentially averaged friction factor based on the local Reynolds number was compared with the experimental result obtained by Cheng and Hwang [29], as shown in Fig. 2. Excellent agreement is found between these two treatments. The above program tests indicate that the adopted solution methods are suitable for the present study.

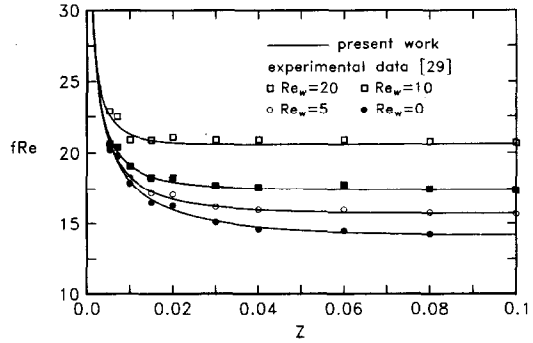

Fig. 2. Comparison of the present predictions and those of Cheng and Hwang [29] for the limiting case.

RESULTS AND DISCUSSION

In this work, the results were presented for air flow ($Pr = 0.7$) in a heated rectangular duct over a wide range of the governing parameters. The wall Reynolds number Re_w are varied from -2 to 4 with Rayleigh numbers Ra ranging from 0 to 2×10^5 for aspect ratios 0.2, 0.5, 1, 2 and 5. Numerical solutions were obtained for the distributions of the velocity, temperature, circumferentially averaged local friction factor and Nusselt number.

Uniform heat flux (UHF)

Figure 3 shows the axial velocity distributions in the cross-section of channel at different axial locations for $Ra = 1 \times 10^5$ in a square duct ($\gamma = 1$) with various values for Re_w in the case of UHF. To assess the influence of buoyancy effects on the mixed convection flow, the results of the limiting case of purely forced convection ($Ra = 0$) are also included in Fig. 3. Since the flow is symmetric with respect to the middle plane ($X = 0.5$), results need only be presented for left half of the duct. An overall inspection on this figure indicates wall transpiration has a considerable influence on the axial velocity distributions. It is well known that the axial velocity profiles for purely forced convection without buoyancy effects are symmetric with respect to the channel axis (i.e. the $Y = 0.5$ line)

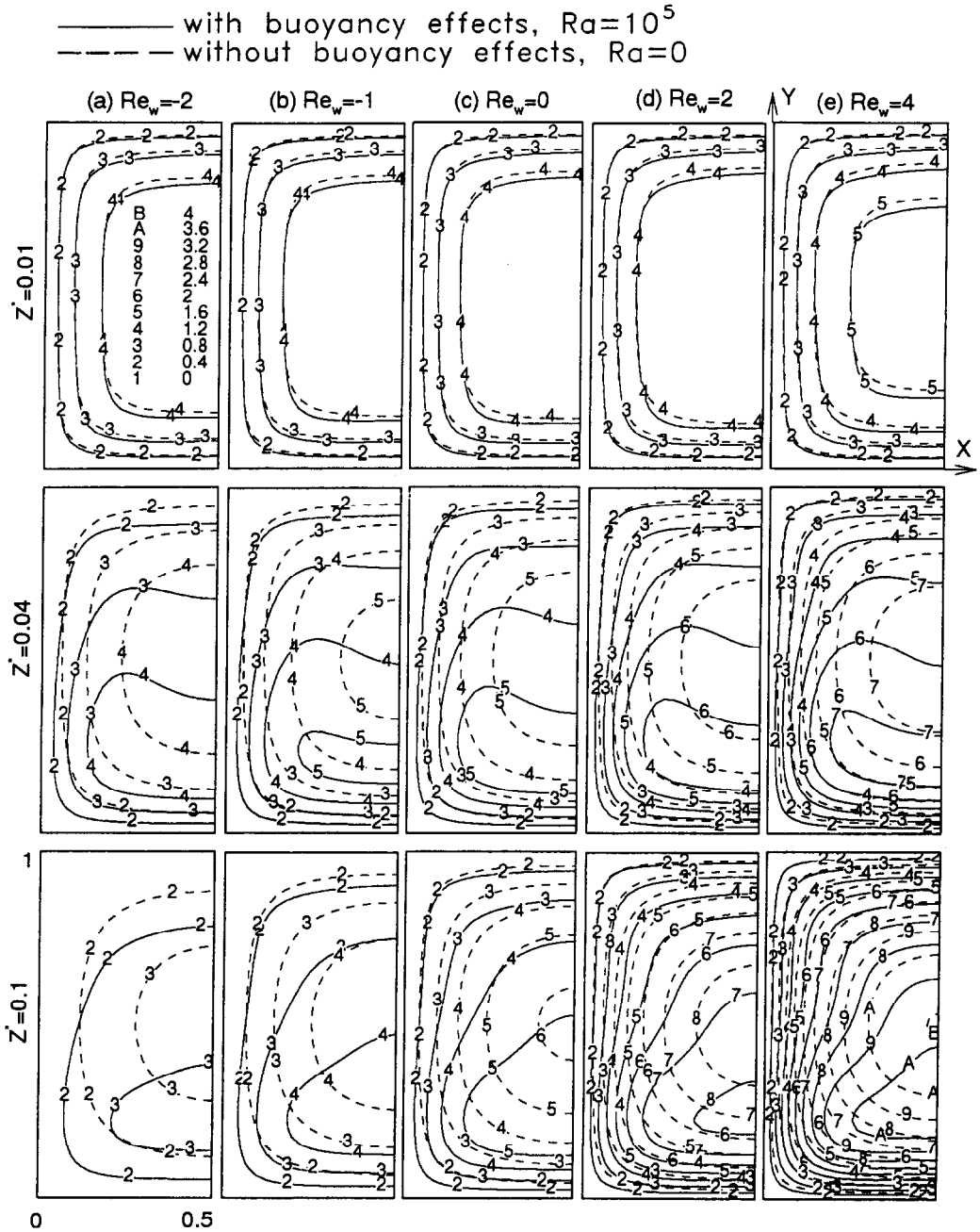

Fig. 3. Effects of Re_w on iso-velocity contours at certain axial locations for UHF case.

through the flow in the duct. Near the entrance ($Z^* = 0.01$), the contours of the axial velocity W in the central core are not shown since the velocity are fairly uniform there. Additionally, the buoyancy effects are still weak and the iso-velocity distributions are seen to be nearly symmetric with respect to the $Y = 0.5$ lines. As the flow moves downstream, the velocity in the core region is accelerated due to the blowing effect for $Re_w > 0$, and decelerated due to the extraction effect for $Re_w < 0$. In the case of purely forced convection, the velocity profiles develop gradually from the uniform distributions at the inlet to the parabolic ones, a situation normally found in laminar internal flow, but as the thermal buoyancy are taken into account, the velocity profiles are distorted by the buoyancy force after a certain axial location and the location of the maximum axial velocity moves toward the bottom horizontal wall ($Y = 0$). Moving away from the inlet, the wall transpiration effect becomes apparent by comparing the maximum W at $Z^* = 0.1$.

The developments of secondary flow is of interest in understanding the flow characteristics and heat transfer mechanism. Figure 4(a)–(c) is the selected results of the buoyancy-induced secondary flow pat-

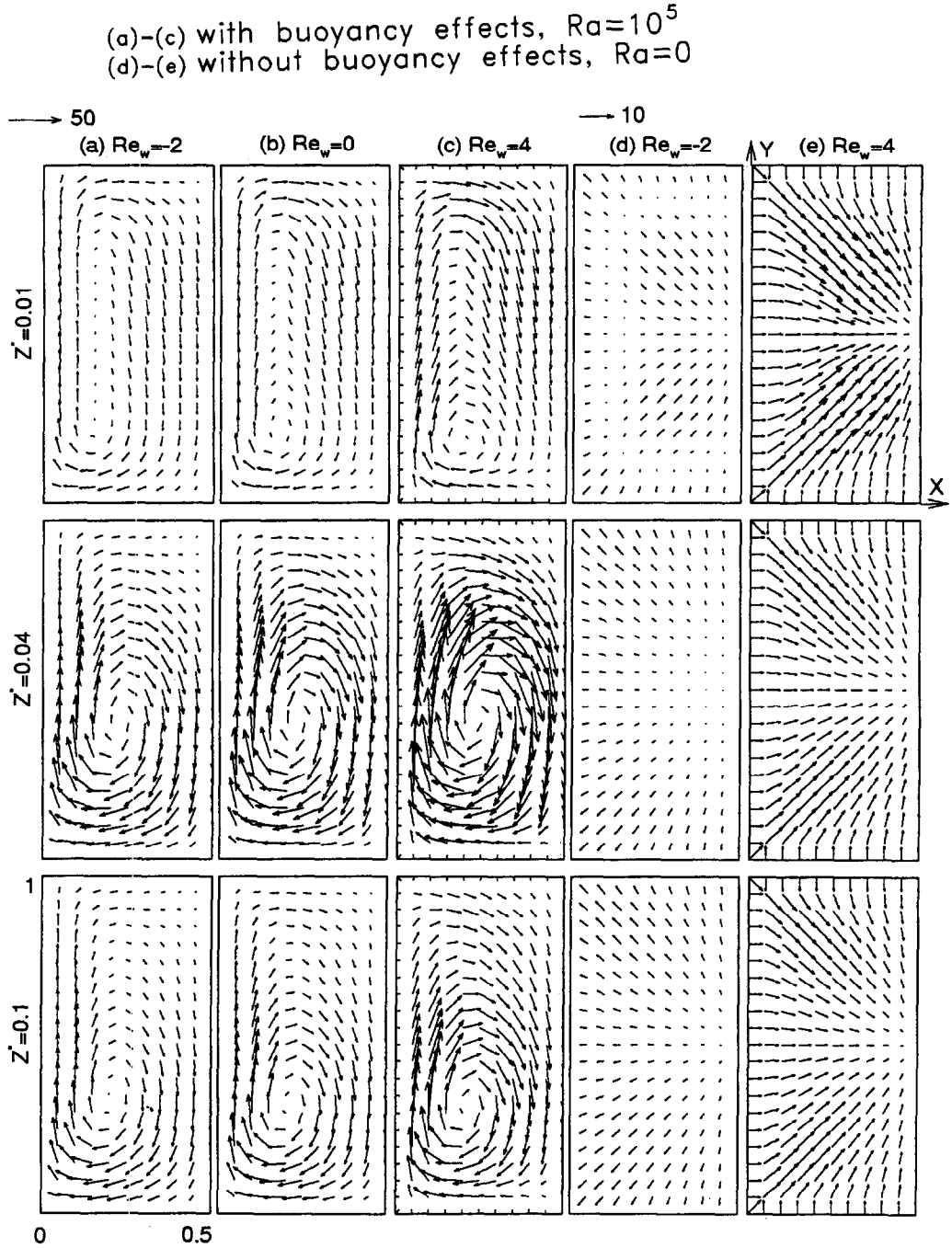

Fig. 4. Effects of Re_w on transverse velocity distribution at certain axial locations for UHF case.

tern in the various cross-sections of the duct for particular values of Re_w. Figure 4(d, e) are the selected results for purely forced convection. As shown in Fig. 4(d) for $Re_w = -2$, near the entrance $Z^* = 0.01$ the velocity vectors near the wall region are radially outward due to the suction effect, but the fluid is squeezed toward the center in the core region by the entrance effect. As the flow goes further downstream ($Z^* = 0.04$), the boundary layer displacement effect is diminished, the fluid in the cross-plane are radially outward. For the case of injection flow $Re_w = 4$ without buoyancy effects [see Fig. 4(e)], the entrance effect causes the increase of inward velocity in the cross-plane, but as the flow moves away from the inlet, the transverse velocity decreases due to the decay of entrance effects. As for the case of mixed convection flow, the buoyancy effects induce an upward flow along the side wall and a downward flow near the central region. Therefore, these flow patterns generate a vortex flow revealed in the cross-section plane. It is also seen that the strength of the vortex becomes stronger when the axial distance Z^* increases from

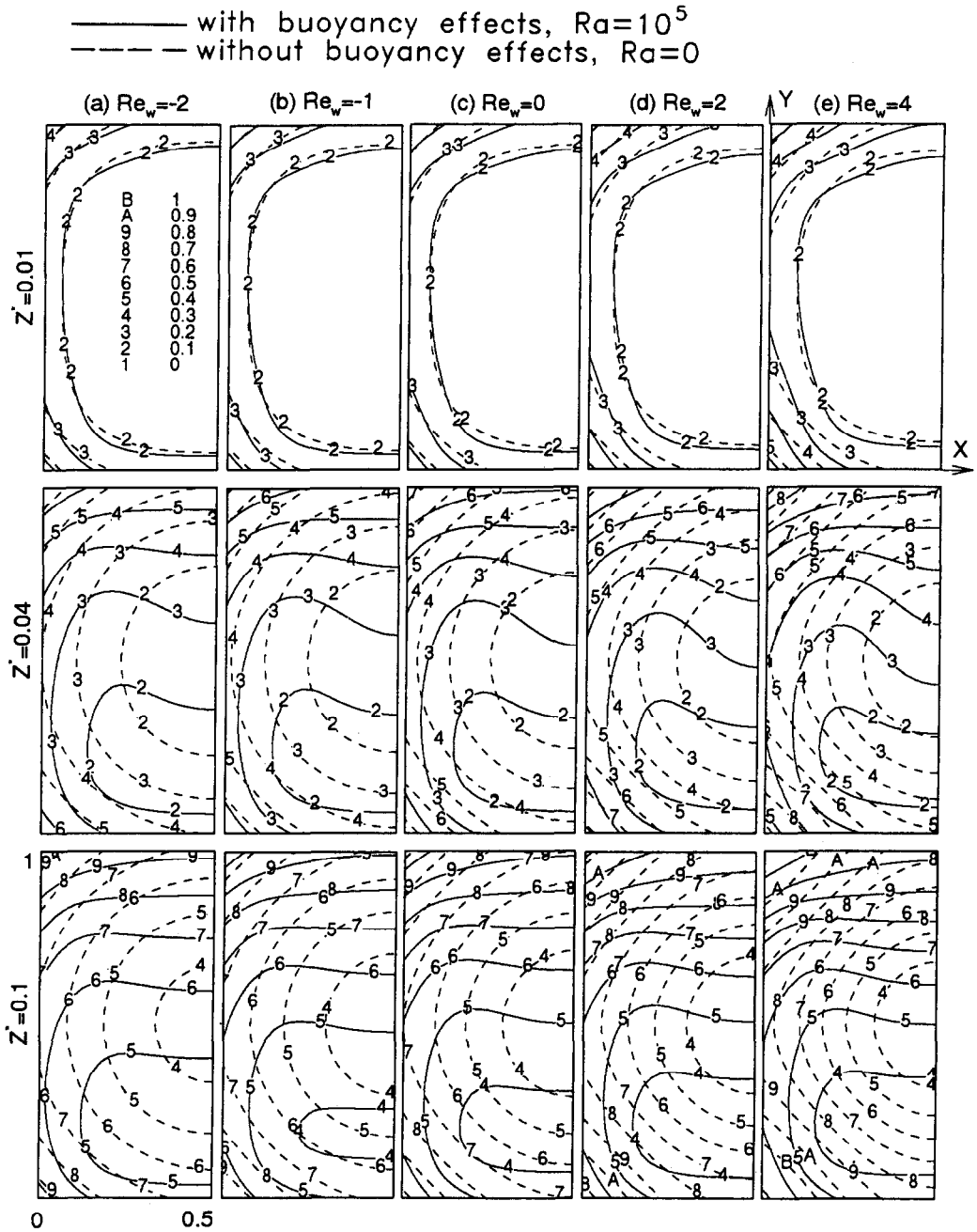

Fig. 5. Effects of Re_w on isotherm contours at certain axial locations for UHF case.

0.01 to 0.04, but as the fluid flows further downstream ($Z^* = 0.1$), the strength of secondary flow becomes weak and the center of the secondary flow moves toward the bottom wall. This phenomenon is attributed to the reduction of the thermal buoyancy effect. Additionally, the strength of secondary flow is stronger for injection case than for suction case. It is also found the separate numerical runs that the maximum transverse velocity vector for $Re_w = 4$ is 105% higher than that for $Re_w = -2$.

Shown in Fig. 5 are the contours of the isotherm at different axial locations. The buoyancy-induced secondary flow carried the fluid heated by the bottom wall, the side wall, and then the top wall. The temperature of the fluid rises higher and higher. But as the flow circulates form the top wall through the center portion to the bottom wall, the fluid is cooled by the upstream fluid. Therefore, the fluid temperatures in the center are lower than those near the side and top walls. It is clear in Fig. 5 that the temperature profiles develop from the case of nearly symmetric with respect to $Y = 0.5$ at $Z^* = 0.01$ to the cases of gradually increasing temperature difference between the top and bottom walls. Notice also that the fluid temperature

near the top wall at any axial locations for injection flow is always higher than that for suction flow. On the contrary, the fluid temperature near the bottom wall is lower for injection flow owing to the stronger convective cooling effect. For the flow without buoyancy effects, the temperature profiles develop symmetrically through the duct. A comparison of the solid and dashed curves indicates that near the bottom wall a lower fluid temperature is noted for the system with consideration of thermal buoyancy effect. Additionally, an opposite behavior is found near the top wall. This is simply due to the thermal buoyancy effects.

Figure 6 presents the axial variations of the circumferentially averaged friction factor fRe and Nusselt number Nu with various wall Reynolds number Re_w. Comparing the solid (with buoyancy effects) and dashed (without buoyancy effects) curves for the corresponding cases indicated that the buoyancy effects on both fRe and Nu are negligible up to a certain distance, but in the further downstream region, the buoyancy effects have a substantial augmentation in both fRe and Nu. In Fig. 6(a), relative to the result of impermeable duct system ($Re_w = 0$), the effects of wall transpiration on the local fRe is slight near the entrance, but as the flow proceeds, fRe increases with increasing axial location for the case of fluid injection ($Re_w > 0$), and the enhancement in fRe due to wall-injection effects increases with an increase in the injection rate. This can be explained by the steeper axial velocity gradient near the duct walls for the stronger injection rate (Fig. 3). The mass extraction ($Re_w < 0$) will decelerate the main stream velocity. Hence the velocity gradient at the duct wall diminishes. This is projected in Fig. 6(a) that the fRe decreases with increasing suction rate Re_w. In Fig. 6(b), the distributions of Nu without buoyancy effect are similar to those of the well-known forced convection flow. That is, the Nu decreases monotonically in the inlet region and then tends to reach a constant fully-developed value. In the presence of buoyancy effects, a local minimum value occurs. This is a result of the combined entrance and buoyancy effects. In addition, a smaller Nu results for a system with a greater injection rate. This is owing to the fact that the wall injection increases the thermal boundary layer thickness and stimulates the fully developed temperature profiles being formed. That is, the temperature difference of the heated wall and the bulk fluid temperature is larger for injection flow, and the injection decreases the axial convection of the heated fluid film compared with both normal convection and axial convection of the impermeable wall. Hence the Nusselt number is smaller for a higher Re_w. On the contrary, the temperature difference is reduced by fluid extraction in the case of suction flow. Hence a higher Nu is obtained with greater suction rate.

For practical applications, the circumferentially averaged wall temperature $\bar{\theta}_w$ and bulk fluid temperature θ_b along the duct are of importance. Figure 7(a, b) give the axial distributions of $\bar{\theta}_w$ and θ_b with the wall Reynolds number Re_w as a parameter. A comparison of corresponding cases of purely forced convection ($Ra = 0$) and mixed convection ($Ra = 10^5$) shows that the results with buoyancy effects have a lower bulk fluid temperature θ_b. It is noted that for the case of injection flow ($Re_w > 0$), higher $\bar{\theta}_w$ and θ_b are observed for a system with a higher Re_w. This can be made plausible by noting the

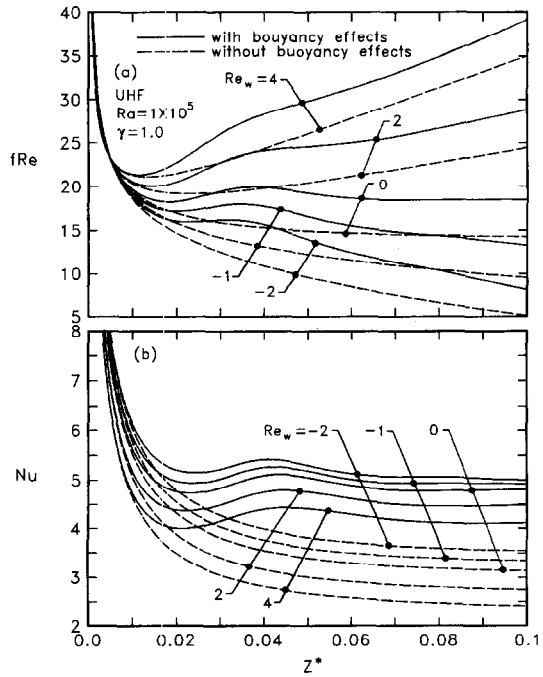

Fig. 6. Effects of Re_w on axial distributions of local averaged friction factor and Nusselt number for UHF case.

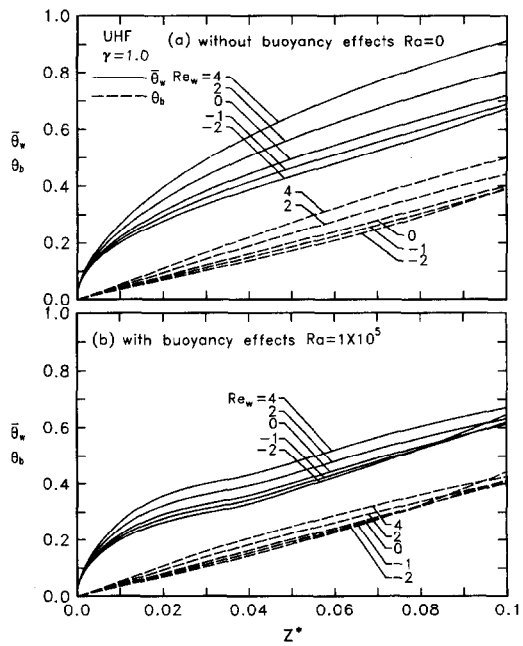

Fig. 7. Effects of Re_w on axial distributions of wall temperature and bulk fluid temperature for UHF case.

fact when the injected fluid with the same temperature as the heated wall is injected into the mainstream, the fluid temperature will be increased. Consequently, the wall temperature θ_w will be affected by the fluid temperature and becomes higher for a higher injection rate Re_w in order to maintain the operating condition of constant heat flux. However, for the case of suction flow ($Re_w < 0$), the distributions of $\bar{\theta}_w$ and θ_b are complicated. Near the entrance region, the $\bar{\theta}_w$ and θ_b decrease with an increase in the suction rate, but as the flow proceeds further downstream, the trend is reverse. This is owing to that fact that the fluid velocity decreases in the downstream region, the transverse conduction becomes the dominant mechanism and the fluid temperature increases rapidly as the location of complete mass extraction is approached.

The effects of the Rayleigh number Ra on the circumferentially averaged friction factor fRe and Nusselt number Nu are presented in Fig. 8(a, b), respectively, for injection ($Re_w = 2$) and suction ($Re_w = -2$) flow. In these two plots, the buoyancy effects are negligible up to a certain axial distance Z^* which depends mainly on the Rayleigh number Ra. This phenomenon can also be seen in the work of Chou and Hwang [32]. The larger the value of Ra, the shorter is this distance. A further investigation reveals that the curves branch out from the curve for purely forced convection (i.e. $Ra = 0$). In the case of injection flow, a local minimum fRe or Nu is the result of the combined entrance and buoyancy effects. After reaching a local minimum value, the curve increases. The occurrence of the local minimum fRe or Nu corresponds to the appearance of the principal pair of vortices. The trends of the distributions of fRe and Nu for the case of suction flow are similar to those of the injection flow, except that the values of fRe are monotonically decreased in the downstream region due to the extraction mass flow. In addition, larger fRe and Nu are noted for a system with a larger Ra due to the stronger buoyancy force. It is worth noting that the free convection effects are practically insignificant for $Ra \leqslant 10^3$. This implies that the forced convection results given by Hwang *et al.* [28, 29] are a limiting case and are applicable only when $Ra \leqslant 10^3$.

The effects of the channel aspect ratio γ on the friction factor fRe are of practical interest. The axial variations of fRe for aspect ratios $\gamma = 0.2$, 0.5, 1, 2 and 5 for both injection and suction flows are shown in Fig. 9(a, b), respectively. In Fig. 9(a), for a given value of γ, a larger fRe is found for a higher Re_w due to a greater mass injection effect, but an opposite trend is found in Fig. 9(b). That is, greater mass extraction effect causes a lower fRe. An overall inspection on Fig. 9 discloses that the curves of low aspect ratio ($\gamma = 0.5$) lies above those of large aspect ratio ($\gamma = 2$) at the same value of Re_w. This is also true for the relationship between the curves of $\gamma = 0.2$ and 5.0. A further comparison of the results reveals that for $\gamma > 1$, a larger value of fRe is obtained for a system with a larger value of γ, but the trend is reversed when $\gamma < 1$.

Wall transpiration effects on the local values of Nu with different values of aspect ratio $\gamma = 0.2$, 0.5, 1, 2 and 5 are shown in Fig. 10. Unlike the effect of Re_w on the local fRe, the Nu is smaller for a higher Re_w due to larger wall-blowing effects. A further comparison of the results in Fig. 10 illustrates that the effect of the aspect ratio on the Nu is appreciable, especially in the

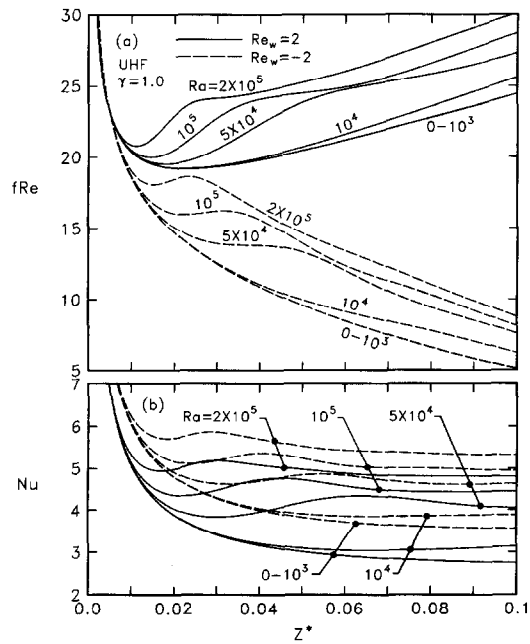

Fig. 8. Effects of Ra on axial distributions of local averaged friction factor and Nusselt number for UHF case.

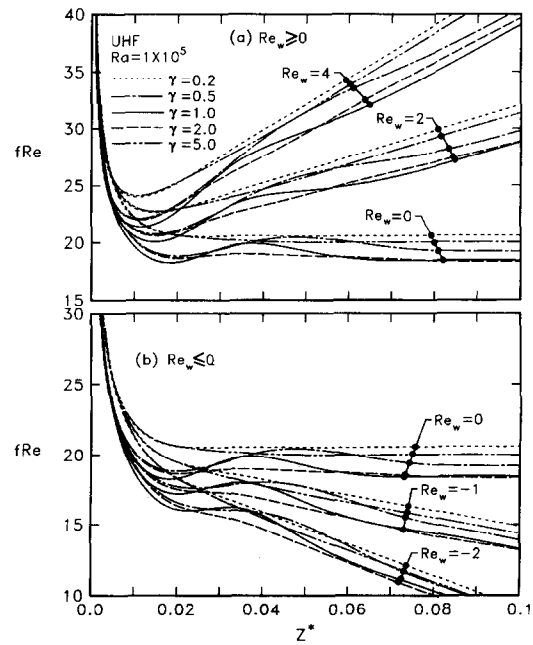

Fig. 9. The variations of local averaged friction factor with Re_w as parameters for various aspect ratios (UHF).

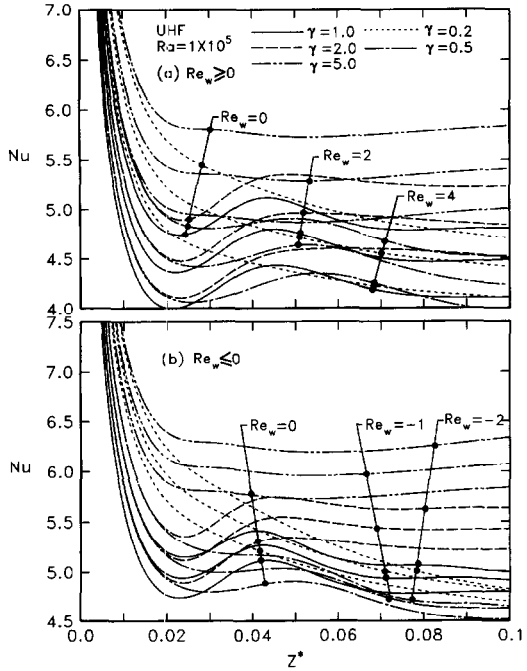

Fig. 10. The variations of local averaged Nusselt number with Re_w as parameters for various aspect ratios (UHF).

downstream region of the duct. It is also noted that the curves for large aspect ratio ($\gamma = 2$) lie above those for small aspect ratio ($\gamma = 0.5$). Similar trend is also found by comparing the distribution of the curves of $\gamma = 5.0$ and $\gamma = 0.2$.

Uniform wall temperature (UWT)

Consideration is now given to the case of UWT. Figure 11 depicts the effects of Re_w on the axial distributions of the local fRe and Nu. In Fig. 11(a), the distribution of fRe is similar to that of the UHF case given in Fig. 6(a). In addition, for the UWT case the discrepancy of fRe between the suction and injection cases is less significant than for the UHF case. In Fig. 11(b), the Nu decreases rapidly to a local minimum value due to the entrance effect. After reaching their minimum values, the Nu increases and reaches a maximum value in the region around $Z^* = 0.02-0.03$. The occurrence of maximum local Nu is closely related to the appearance of local maximum secondary flow intensity [32, 33]. After that, with the decay of the secondary flow, the Nu decreases monotonically with increasing axial distance. It is also interesting to note that, relative to the case of $Re_w = 0$, the wall injection would reduce the Nu. In the case of mass extraction ($Re_w < 0$), the opposite trend occurs. The Nu increases with increasing suction wall Reynolds number. Additionally, the Nusselt number Nu is higher for the UWT case than that for UHF case at the same Re_w (comparing Figs 6 and 11).

The effects of aspect ratio γ on the distributions of local Nu are illustrated in Fig. 12. It is noted that the influences of aspect ratio are more significant in the UWT case. In Fig. 12, a minimum local Nu appears at a specified distance from the entrance which depends upon the values of Re_w for the case of $\gamma \leqslant 1$. After reaching the local minimum point, the variation of Nu shows an increase to a maximum value. A careful comparison of the variations of Nu between the curves of $\gamma = 0.2$ and 5.0 in the downstream region discloses that the slender duct ($\gamma = 0.2$) shows a higher Nu than the wider duct ($\gamma = 5.0$) does. A similar relationship in the Nu between $\gamma = 0.5$ and 2 is also observed. This is owing to the stronger secondary flow induced by

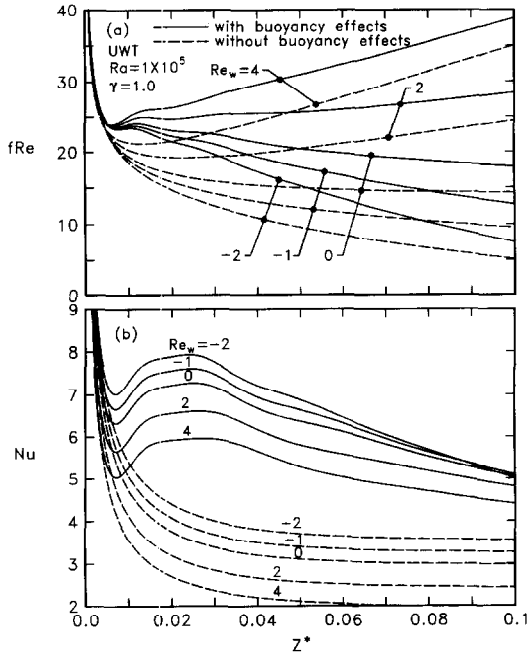

Fig. 11. Effects of Re_w the axial variations of local averaged friction factor and Nusselt number for UWT case.

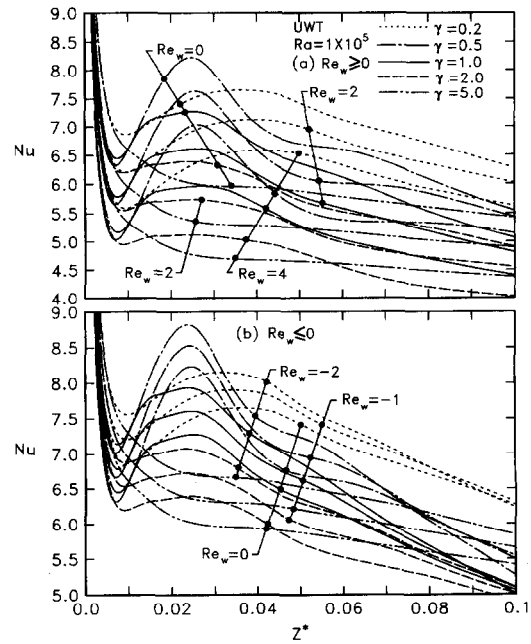

Fig. 12. The variations of local averaged Nusselt number with Re_w as parameters for various aspect ratios (UWT).

thermal buoyancy for the slender duct, but in the case of UHF (Fig. 10), the trend is reversed, i.e. a lower Nu is observed for a slender duct. It is believed that for the UHF cases, the averaged temperature difference between the duct wall temperature and bulk fluid temperature is increased to maintain the uniform wall heat flux. Hence a lower Nu can be resulted for a smaller γ according to the definition of Nu in equation (15).

Correlations of longitudinal averaged friction factor and Nusselt number

To facilitate the applications of the above result, correlating equations for the longitudinal averaged friction factor and Nusselt number for both boundary conditions in the entrance region up to $Z^* = 0.1$ are given here.

Uniform heat flux (UHF)

$$\frac{\overline{Nu}}{\overline{Nu_0}} = \bar{a}+\bar{b}\cdot\exp(2.45\log Ra) + \bar{c}\cdot(\log Ra)^{1.5}+\bar{d}\cdot(\log Ra)^{7}\cdot Re_w \quad (18)$$

$$\frac{\overline{fRe}}{\overline{fRe_0}} = \bar{a}+\bar{b}\cdot\exp(2.5\log Ra) + \bar{c}\cdot(\log Ra)^{1.5}+\bar{d}\cdot(\log Ra)^{5}\cdot Re_w. \quad (19)$$

Uniform wall temperature (UWT)

$$\frac{\overline{Nu}}{\overline{Nu_0}} = \bar{a}+\bar{b}\cdot\exp(2.85\log Ra) + \bar{c}\cdot(\log Ra)^{1.6.6}+\bar{d}\cdot(\log Ra)^{7}\cdot Re_w \quad (20)$$

$$\frac{\overline{fRe}}{\overline{fRe_0}} = \bar{a}+\bar{b}\cdot\exp(2.5\log Ra) + \bar{c}\cdot(\log Ra)^{1.4.5}+\bar{d}\cdot(\log Ra)^{5}\cdot Re_w \quad (21)$$

where constants $\bar{a}$, $\bar{b}$, $\bar{c}$ and $\bar{d}$ are listed in Table 2. In the above equations, $\overline{fRe_0}$ and $\overline{Nu_0}$ represent the longitudinal averaged friction factor and Nusselt number, respectively, without buoyancy effects ($Ra = 0$). They are correlated as follows:

$$\overline{fRe_0}, \overline{Nu_0} = \bar{e}+\bar{f}\cdot Re_w \quad (22)$$

where constants $\bar{e}$ and $\bar{f}$ are also listed in Table 2. Constant $\bar{e}$ is the value of $\overline{fRe_0}$ and $\overline{Nu_0}$ for impermeable duct flow ($Re_w = 0$). Equations (19–21) are correlated within 5% for $-2 < Re_w < 4$ and $Ra \leqslant 2\times 10^5$.

CONCLUDING REMARKS

The characteristics of mixed convection flow and heat transfer in horizontal rectangular ducts with wall transpiration effects have been studied numerically. A relative novel vorticity–velocity method successively solved the three-dimensional parabolic governing equations. The effects of the wall Reynolds number Re_w, Rayleigh number Ra and aspect ratio γ on the flow and heat transfer are investigated in detail by examining the local flow structure and temperature fields. The major conclusions of the work can be drawn as follows:

(1) At the very beginning of the inlet region, the cross-flows are all directed toward the center of the duct. As the flow moves downstream, the flow reorganizes and a secondary flow develops due to the presence of the thermal buoyancy. At downstream region ($Z^* = 0.1$), the secondary flow is stronger for the case with a greater injected rate ($Re_w = 4$).

(2) The variations of the friction factor fRe and the Nusselt number Nu are characterised by a drop near the inlet due to the entrance effect; but the decay is attenuated by the onset of secondary flow.

(3) For injection case ($Re_w > 0$), the Nusselt number Nu is retarded with an increase in the wall Reynolds number Re_w, but the trend is reverse for the effect of Re_w on the fRe.

(4) A larger value of fRe is observed for a system with a larger γ, provided that $\gamma > 1$, but the trend is reverse for $\gamma < 1$.

(5) Under the range of parameters investigated, the thermal buoyancy effect is negligible only when $Ra \leqslant 10^3$.

Table 2. Constants of the correlating equations of average friction factors and Nusselt numbers

	UHF						UWT					
	$\bar{a}$	$\bar{b}\times 10^7$	$\bar{c}\times 10^{12}$	$\bar{d}\times 10^7$	$\bar{e}$	$\bar{f}$	$\bar{a}$	$\bar{b}\times 10^7$	$\bar{c}\times 10^{12}$	$\bar{d}\times 10^7$	$\bar{e}$	$\bar{f}$
γ						$\overline{Nu}/\overline{Nu_0}$						
0.2	0.9906	11.09	−4.596	2.148	5.244	−0.2490	0.9732	5.897	−1.516	3.850	5.588	−0.3042
0.5	0.9764	36.61	−17.51	2.514	4.366	−0.2183	0.9716	23.13	−7.131	8.037	4.221	−0.2785
1.0	0.9796	50.62	−24.68	2.349	4.151	−0.1996	1.014	25.03	−7.743	9.827	3.789	−0.2752
2.0	0.9799	55.88	−27.38	2.100	4.366	−0.2183	1.001	1.518	−4.693	4.682	4.221	−0.2785
5.0	0.9864	32.60	−15.59	1.518	5.256	−0.2440	0.9954	2.770	−0.7810	1.011	5.578	−0.3036
						$\overline{fRe}/\overline{fRe_0}$						
0.2	0.9967	3.885	−1.697	−17.62	20.50	2.816	0.9873	17.97	−24.55	−41.64	20.52	2.824
0.5	0.9848	23.62	−15.02	−54.18	17.67	2.673	0.9838	54.54	−85.75	−105.4	17.67	2.673
1.0	0.9927	30.03	−19.50	−75.44	16.64	2.629	0.9975	60.41	−95.48	−135.7	16.65	2.631
2.0	0.9958	17.51	−11.19	−43.40	17.67	2.673	0.9940	35.29	−54.37	−80.71	17.67	2.673
5.0	0.9987	3.731	−2.203	−10.53	20.56	2.831	0.9978	6.097	−7.903	−20.40	20.56	2.830

(6) The buoyancy effects on the present problem are more significant for UWT case than for UHF case.

Acknowledgement—The financial support of this work by the National Science Council, Republic of China, through the contract NSC84-2212-E-211-003 is greatly appreciated.

REFERENCES

1. Berman, A. S., Laminar flow in channels with porous walls. *Journal of Applied Physics*, 1953, **24**, 1232–1235.
2. Donoughe, P. L., Analysis of laminar incompressible flow in semi-porous channels. NASA TN3759, NACA, 1956.
3. Carter, L. F. and Gill, W. N., Asymptotic solution for combined free and forced convection in vertical and horizontal conduits with uniform suction and blowing. *AIChE Journal*, 1964, **10**, 330–339
4. Terrill, R. M., Heat transfer in laminar flow between parallel porous plates. *International Journal of Heat and Mass Transfer*, 1965, **8**, 1491–1497.
5. Yeroshenko, V. M., Zaichik, L. I. and Bakhvalov, B. Yu, Heat transfer in laminar plane channel flow with uniform suction or injection. *International Journal of Heat Transfer*, 1981, **24**, 1649–1655.
6. Doughty, J. R., and Perkins, H. C., Jr, The thermal entry problem for laminar flow between parallel porous plates. *ASME Journal of Heat Transfer*, 1971, **93**, 476–478.
7. Doughty, J. R. and Perkins, H. C., Jr, Thermal and combined entry problems for laminar flow between parallel porous plates. *ASME Journal of Heat Transfer*, 1972, **94**, 233–234.
8. Doughty, J. R. and Perkins, H. C., Jr, Variable properties laminar gas flow heat transfer in the entry region of parallel porous plates. *International Journal of Heat and Mass Transfer*, 1973, **16**, 663–668.
9. Raithby, G. D. and Knudsen, D. C., Hydrodynamic development in a duct with suction and blowing. *ASME Journal of Applied Mechanics*, 1974, **96**, 896–902.
10. Tsou, R. C. H. and Chang, Y. P., On the linearized analysis of entrance flow in heated porous conduits. *International Journal of Heat and Mass Transfer*, 1976, **19**, 445–458.
11. Rhee, S. J. and Edwards, D. K., Laminar entrance flow in a flat plate duct with asymmetric suction and heating. *Numerical Heat Transfer*, 1981, **4**, 85–100.
12. Lessner, P. and Newman, J., Hydrodynamics and mass transfer in a porous-wall channel. *Journal of the Electrochemical Society*, 1984, **131**, 1828–1831.
13. Sorour, M. M., Hassab, M. A. and Estafanous, S., Developing laminar flow in a semi-porous two-dimensional channel with nonuniform transpiration. *International Journal of Heat and Fluid Flow*, 1987, **8**, 44–54.
14. Yuan, S. W. and Finkelstein, A. B., Laminar pipe flow with injection and suction through a porous wall. *ASME Journal of Heat Transfer*, 1956, **78**, 719–724.
15. Olson, R. M. and Eckert, E. R. G., Experimental studies of turbulent flow in a porous circular tube with uniform fluid injection through the tube wall. *Journal of Applied Mechanics*, 1966, **33**, 7–17.
16. Kinney, R. B., Fully developed frictional and heat transfer characteristics of laminar flow in porous tubes. *International Journal of Heat and Mass Transfer*, 1968, **11**, 1393–1401.
17. Bundy, R. D. and Weissberg, H. L., Experimental study of fully developed laminar flow in a porous pipe with wall injection. *Physics of Fluids*, 1970, **13**, 2613–2615.
18. Yeroshenko, V. M., Yershov, A. V. and Zaichik, L. I., Calculation of fully developed turbulent flow in a tube with injection and suction. *High Temperature*, 1981, **13**, 80–85.
19. Yeroshenko, V. M., Ershov, A. V. and Zaichik, L. I., Heat transfer for turbulent flow in a circular tube with uniform suction and injection. *International Journal of Heat and Mass Transfer*, 1984, **27**, 1197–1203.
20. Hirata, Y. and Ito, R., Extension of the mixing length theory to a porous tube flow with injection or suction. *Journal of Chemical Engineering Japan*, 1982, **15**, 452–458.
21. Yuan, S. W. and Finkelstein, A. B., Heat transfer in laminar pipe flow with uniform coolant injection. *Jet Propulsion*, 1958, **28**, 178–181.
22. Pederson, R. J. and Kinney, R. B., Entrance-region heat transfer for laminar flow in porous tubes. *International Journal of Heat and Mass Transfer*, 1971, **14**, 159–161.
23. Raithby, G. D., Laminar heat transfer in the thermal entrance of circular tubes and two-dimensional rectangular ducts with wall suction and injection. *International Journal of Heat and Mass Transfer*, 1971, **14**, 224–243.
24. Raithby, G. D., Heat transfer in tubes and ducts with wall mass transfer. *Canadian Journal of Chemical Engineering*, 1972, **50**, 456–461.
25. Hirata, Y., Komatsu, S. and Ito, R., Experimental study of flow development in a porous tube with injection or suction. *Journal of Chemical Engineering Japan*, 1982, **15**, 455–451.
26. Faghri, A., Heat-transfer characteristics in annuli with blowing or suction at the walls. *Journal of Thermophysics and Heat Transfer*, 1990, **4**, 59–66.
27. Raptis, A., Mani, J. P. and Prasad, S., Steady flow of a viscous incompressible fluid between two co-axial circular cylinder with suction and injection. *Warme-und Stoffubertrangung*, 1993, **29**, 56–61.
28. Hwang, G. J., Cheng, Y. C. and Ng, M. L., Developing laminar flow and heat transfer in a square duct with one-walled injection and suction. *International Journal of Heat and Mass Transfer*, 1993, **36**, 2429–2440.
29. Cheng, Y. C. and Hwang, G. J., Experimental study of laminar flow and heat transfer in a one-porous-wall square duct with wall injection. *International Journal of Heat and Mass Transfer*, 1995, **38**, 3475–3484.
30. Incropera, F. P. and Schutt, J. A., Numerical simulation of laminar mixed convection in the entrance region of horizontal rectangular ducts. *Numerical Heat Transfer*, 1985, **8**, 707–729.
31. Incropera, F. P., Knox, A. L. and Schutt, J. A., Mixed convection flow and heat transfer in the entry region of a horizontal rectangular duct. *ASME Journal of Heat Transfer*, 1987, **109**, 434–439.
32. Chou, F. C. and Hwang, G. J., Vorticity–velocity method for the Graetz problem and the effect of natural convection in a horizontal rectangular channel with uniform wall heat flux. *ASME Journal of Heat Transfer*, 1987, **109**, 704–710.
33. Lin, J. N., Chou, F. C., Yan, W. M. and Tzeng, P. Y., Combined buoyancy effects of thermal and mass diffusion on laminar forced convection in the thermal entrance region of horizontal square duct. *Canadian Journal of Chemical Engineering*, 1992, **70**, 681–689.
34. Lin, J. N., Tzeng, P. Y., Chou, F. C. and Yan, W. M., Convective instability of heat and mass transfer for laminar forced convection in the thermal entrance region of horizontal rectangular channels. *International Journal of Heat and Fluid Flow*, 1992, **13**, 250–280.
35. Shah, R. K. and London, A. L., *Laminar Flow Forced Convection in Duct*. Academic Press, New York, 1978.
36. Ramakrishna, K., Rubin, S. G. and Khosla, P, K., Laminar natural convection along vertical square ducts. *Numerical Heat Transfer*, 1982, **5**, 59–79.
37. Roche, P. J. *Computational Fluid Dynamics*. Reinhold, New York, 1971, pp. 61–64.